

Journal of Materials Chemistry C

Accepted Manuscript



This is an *Accepted Manuscript*, which has been through the Royal Society of Chemistry peer review process and has been accepted for publication.

Accepted Manuscripts are published online shortly after acceptance, before technical editing, formatting and proof reading. Using this free service, authors can make their results available to the community, in citable form, before we publish the edited article. We will replace this *Accepted Manuscript* with the edited and formatted *Advance Article* as soon as it is available.

You can find more information about *Accepted Manuscripts* in the [Information for Authors](#).

Please note that technical editing may introduce minor changes to the text and/or graphics, which may alter content. The journal's standard [Terms & Conditions](#) and the [Ethical guidelines](#) still apply. In no event shall the Royal Society of Chemistry be held responsible for any errors or omissions in this *Accepted Manuscript* or any consequences arising from the use of any information it contains.

The effect of surface ligand, solvent and Yb³⁺ co-doping on luminescence properties of Er³⁺ in colloidal NaGdF₄ nanocrystals

J. Cichos¹, L. Marciniak², D. Hreniak^{2,*}, W. Strek², M. Karbowski^{1,*}

¹*Faculty of Chemistry, University of Wrocław, 50-383 Wrocław, Poland*

**Miroslaw.Karbowski@chem.uni.wroc.pl*

²*Institute of Low Temperature and Structure Research, Polish Academy Sciences, 50-422 Wrocław, Poland*

**D.Hreniak@int.pan.wroc.pl*

Abstract

The emission properties of NaGdF₄ nanoparticles (NPs) doped with Er³⁺ and/or Yb³⁺ ions and their colloidal dispersions in different solvents were investigated. The organic ligands present on the NPs surface decrease the decay time of Er³⁺ emission. In contrast, virtually no change in decay times was observed after dispersing the NPs in solvents. Both surface ligands and solvent molecules exert a pronounced effect on the intensity ratio of ²H_{11/2}+⁴S_{3/2}→⁴I_{15/2} and ⁴F_{9/2}→⁴I_{15/2} transitions. Co-doping with Yb³⁺ is revealed as another important factor influencing relative intensities of Er³⁺ emission bands. The influence of surface ligands and solvent molecules on emission spectra upon NIR excitation at 980 nm was investigated. The decay times of Er³⁺ emission are longer for Yb³⁺ co-doped NPs than for analogous NPs single doped with Er³⁺. This is ascribed to a feedback energy transfer process between Yb³⁺ and Er³⁺.

1. Introduction

Up-converting bio-functionalized and water soluble nanoparticles (NPs) show a great promise for use as luminescent probes in medical imaging. According to the technological forecasts they will play an important role in modern bio-assays in forthcoming years [1-6.]. The excitation with near infrared (NIR) radiation increases their possible application viability because of low tissue autofluorescence level and good penetration depth of light in the so-called therapeutic window. One of the most important classes of compounds for such applications are different types of lanthanide doped fluoride nanocrystals, which can both efficiently convert near-infrared light to visible light (up-conversion process) and, additionally, exhibit magnetic properties due to the presence of gadolinium ions. An example of such bifunctional host lattice is the hexagonal Er³⁺ and Yb³⁺ co-doped NaGdF₄ crystal [7-12]. Very high efficiency of emission in such fluorides is due to the low phonon energy resulting in decrease of nonradiative multiphonon transition rates, the high disorder structure due to cation (Na⁺) distribution, the resonant energy transfer between Yb³⁺(²F_{5/2}) and Er³⁺(⁴I_{11/2}) levels [13] and by

possibility of manipulation of the spatial distributions of these dopant ions in core-shell structures [14,15]. Another important criterion for choosing a suitable material is limited agglomeration and facility of functionalization of surface of separated nanocrystals. Strategy for the sensitization and protection of luminescence of rare-earth-doped nanocrystals has also a great importance for the final biomedical applications. Several different preparation methods of nanosized up-converting fluorides offering such capabilities were reported recently [16-24].

Recently, systematic studies of the solvent effect on luminescence properties of Nd^{3+} doped NaYF_4 nanocrystals dispersed in several nonpolar liquids were reported [21]. The authors have observed an evident relationship between optical properties and the effective refractive index of the host liquid medium. Other authors reported differences of the colour emission ratio for the upconversion luminescence of oleate-capped $\text{NaYF}_4:\text{Yb}^{3+}/\text{Er}^{3+}$ nanoparticles dispersed in toluene compared to ligand free $\text{NaYF}_4:\text{Yb}^{3+}/\text{Er}^{3+}$ nanoparticles dispersed in water [25]. Organic ligands present on the surface of the nanocrystals may exert even more pronounced effect on their luminescence properties.

The main aim of the present work was to investigate the influence of surface ligands on luminescence properties of $\text{NaGdF}_4:\text{Yb}^{3+},\text{Er}^{3+}$ nanocrystals, both in solid state and colloiddally dispersed in different solutions. Moreover, the effect of Yb^{3+} co-doping was also investigated. In spite of many studies on this material, there have been no systematic investigations explaining how their luminescence properties are affected by surface modifications and the surroundings of the nanocrystals. In order to prevent agglomeration of the nanocrystals we have chosen oleic acid (OA) and polyethylene glycol (PEG)-phosphate as ligands. OA is a capping ligand which is used in the most successful and widely employed method of synthesis of NaLnF_4 nanocrystals. OA may be easily exchanged to (PEG)-phosphate that was found to be non-cytotoxic and is already used in pharmaceutical applications [26]. The organic ligand-free control sample was obtained by removing OA using NOBF_4 [27].

2. Experimental

The synthesis of OA-capped NaGdF_4 ($\text{NaGdF}_4@\text{OA}$) nanoparticles singly doped with Er^{3+} (2%) or co-doped with Yb^{3+} (18%) and Er^{3+} (2%) ions was carried out by thermolysis of trifluoroacetates in mixture of oleic acid and octadecene [1]. PEG-phosphate synthesis (α -methoxy- ω -phosphate poly(ethylene glycol)) and ligand exchange method (yielding $\text{NaGdF}_4@\text{PEG}$ NPs) were described previously by van Veggels and co-workers [28]. The organic ligand-free NPs ($\text{NaGdF}_4@\text{BF}_4$) were obtained following the procedure described in [27,29]. The XRD patterns were measured on a Bruker D8 Advance diffractometer equipped with Cu lamp and Vantec detector. In order to compare spectroscopic properties of colloidal solutions of fluorides, the nanocrystals were diluted in the same concentration in each of the solvents. The luminescence spectra were recorded using a Jobin-Yvon HR1000 monochromator supplied with a CCD camera. The upconversion (UC) emission spectra were

measured under 976 nm light from a laser diode. The decay profiles were collected using a LeCroy WaveSurfer 400 oscilloscope and the 976 nm line of a Ti:Sapphire laser or Edinburgh Instruments FLSP 920 spectrofluorimeter and 377 nm light of microsecond pulsed xenon flashlamp.

3. Results and discussion

3.1. Morphology characterization

The $\text{NaGdF}_4:\text{Yb}^{3+},\text{Er}^{3+}$ nanocrystals capped with OA or functionalized with PEG-phosphate ligands are easily dissolved in different solvents forming stable colloidal solutions. The XRD patterns prove the phase purity of the obtained NCs and confirm that all the synthesized NCs are hexagonal phase (PDF #270699). The nanocrystals were characterized by TEM measurements. The respective images (Fig. 1a,b) clearly show nonaggregated particles. The average size of OA coated nanocrystals was determined to be 22 nm. After exchange of OA with PEG-phosphate ligand the average size increases to 27 nm, but the size distribution remains relatively narrow (Fig. 1c).

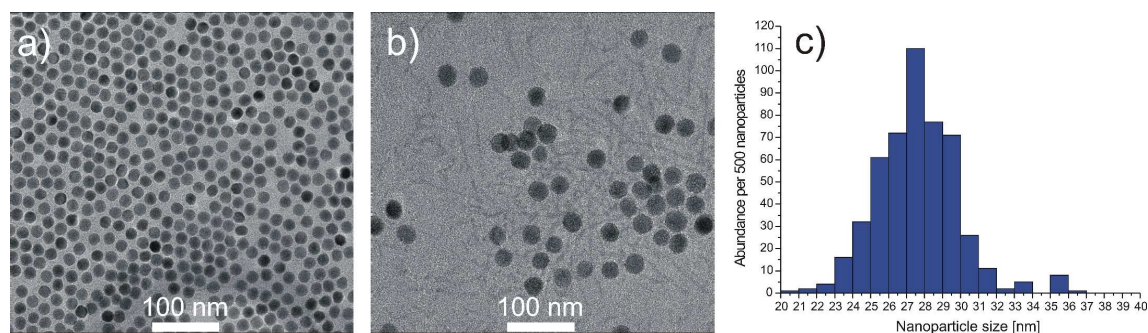


Figure 1. TEM images of a) $\text{NaGdF}_4:\text{Yb}^{3+},\text{Er}^{3+}@OA$ and b) $\text{NaGdF}_4:\text{Yb}^{3+},\text{Er}^{3+}@PEG$ NPs and c) size distribution of $\text{NaGdF}_4:\text{Yb}^{3+},\text{Er}^{3+}@PEG$.

3.2. Emission spectra

Figure 2 presents the emission spectra recorded for $\text{NaGdF}_4:\text{Er}^{3+}(2\%)@BF_4$ and $\text{NaGdF}_4:\text{Er}^{3+}(2\%),\text{Yb}^{3+}(18\%)@BF_4$ samples under excitation at 377 nm (the $^4G_{11/2}$ multiplet). Nitrosonium tetrafluoroborate removes OA or other organic ligands from the NPs surface. If such surface ligands are present an additional broad band is observed in emission spectra in the 400 – 550 nm range [27]. Three groups of bands can be distinguished in the spectra in Fig. 2. The blue band at 407 nm is attributed to the $^2H_{9/2} \rightarrow ^4I_{15/2}$ transition. The green emission bands at 540 and 520 nm are due to de-excitation of $^4S_{3/2}$ and thermalized $^2H_{11/2}$ levels, respectively. At about 654 nm the red $^4F_{9/2} \rightarrow ^4I_{15/2}$ emission is observed. The weak band at ~700 nm is attributed to the $^2H_{9/2} \rightarrow ^4I_{11/2}$ transition, whereas transition from $^2H_{9/2}$ to $^4I_{13/2}$ levels gives rise to the peak observed in the green emission band at ~556 nm.

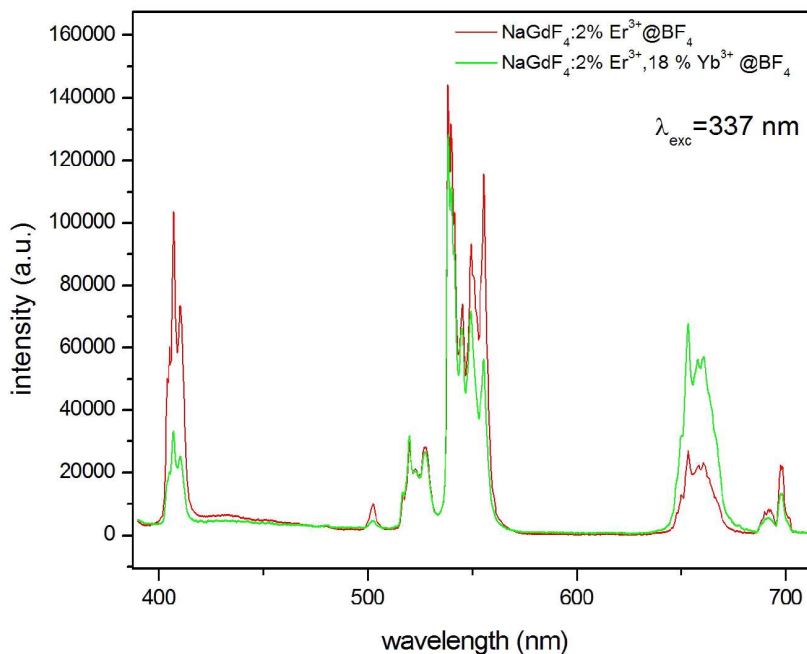


Fig. 2. Emission spectra recorded for NaGdF₄:Er³⁺(2%)@BF₄ (a) and NaGdF₄:Er³⁺(2%),Yb³⁺(18%)@BF₄ (b) solid samples under direct excitation at 377 nm.

The highest phonon energy of the NaLnF₄ host is about 500 cm⁻¹. The energy differences between the emitting ⁴S_{3/2} or ⁴F_{9/2} levels and subsequent lower energy levels is more than 3000 cm⁻¹, which means that at least six phonons are required to bridge this energy gap. Therefore, for a free of surface ligands microscopic sample obtained by a solid state reaction, participation of multiphonon relaxation in deactivation of the ⁴S_{3/2} or ⁴F_{9/2} levels is insignificant. This implies that the decay time of the ⁴F_{9/2} level which is not deactivated via cross-relaxation processes, is only slightly temperature dependent. For NaYF₄:Er³⁺(2%) (NaYF₄:Er³⁺(2%),Yb³⁺(18%)) micropowders the measured decay times are 0.6(0.55) and 0.43(0.47) ms at 5 K and 300 K, respectively [13]. In contrast, the ⁴S_{3/2} level is strongly deactivated by cross-relaxation processes, especially in samples doped with higher concentration of Er³⁺. The decay times reported for the microscopic NaYF₄ samples doped with Er³⁺ at 2% and 20 % are 0.36 and 0.026 ms, respectively [13].

As particle sizes decrease to a nanometer size range, the ligands present at the surface start to play an important role in deactivation processes, owing to increase of the surface-to-volume ratio. The decay times of NPs capped with different surface ligands, measured for solids samples or nanoparticle colloidal dispersions in different solvents, are listed in Table 1.

Table 1. Decay times (in μs) of emission bands in $\text{NaGdF}_4:\text{Er}^{3+}(2\%)$ and $\text{NaGdF}_4:\text{Er}^{3+}(2\%),\text{Yb}^{3+}(18\%)$ NPs capped with different ligands measured upon a direct excitation at 377 nm for solid samples and their colloidal dispersions.

sample	$\text{Er}^{3+}(2\%)$			$\text{Er}^{3+}(2\%),\text{Yb}^{3+}(18\%)$		
	${}^2\text{H}_{9/2} \rightarrow {}^4\text{I}_{15/2}$ (407 nm)	${}^4\text{S}_{3/2} \rightarrow {}^4\text{I}_{15/2}$ (540 nm)	${}^4\text{F}_{9/2} \rightarrow {}^4\text{I}_{15/2}$ (654 nm)	${}^2\text{H}_{9/2} \rightarrow {}^4\text{I}_{15/2}$ (407 nm)	${}^4\text{S}_{3/2} \rightarrow {}^4\text{I}_{15/2}$ (540 nm)	${}^4\text{F}_{9/2} \rightarrow {}^4\text{I}_{15/2}$ (654 nm)
$\text{NaGdF}_4@\text{OA}$ powder	22	101	144	22	183	247
$\text{NaGdF}_4@\text{OA}$ in toluene	22	110	143	20	188	231
$\text{NaGdF}_4@\text{BF}_4$ powder	25	74	153	25	156	271
$\text{NaGdF}_4@\text{PEG}$ powder	19	75	98	20	135	165
$\text{NaGdF}_4@\text{PEG}$ in water	21	67	114	18	124	186

The decay times listed in Table 1 are significantly shorter than those for the solid state synthesized microscopic sample (e.g. 0.43 ms and 0.47 ms for ${}^4\text{F}_{9/2} \rightarrow {}^4\text{I}_{15/2}$ transition in $\text{NaYF}_4:\text{Er}^{3+}(2\%)$ and $\text{NaYF}_4:\text{Er}^{3+}(2\%),\text{Yb}^{3+}(18\%)$, respectively [13]) and depend on the kind of ligand present on the surface. This implies that in the presence of OA or other surface ligands with highly energetic ($\sim 3500\text{ cm}^{-1}$) OH vibrations the emitting levels, including ${}^4\text{F}_{9/2}$, are de-excited through multiphonon relaxation processes. The shortest decay time is observed for NPs functionalized with PEG-phosphate ligands. There is virtually no change in the lifetime after dispersing of OA capped NPs in toluene. The highest energy vibrations of toluene molecules are alkyl and aromatic C-H stretches that occur at $2900\text{--}3100\text{ cm}^{-1}$. OA possesses high energy vibrations in a similar range, i.e. at $\sim 3000\text{ cm}^{-1}$. Therefore, the increase of multiphonon relaxation rates is not expected for $\text{NPs}@\text{OA}$ colloidal dispersion in toluene. In fact, a small elongation of decay times is observed, which may result from removal of water molecules and/or hydroxyl groups present at the NPs surface, as is evidenced by a water absorption broad band observed in the $3000\text{--}3600\text{ cm}^{-1}$ region in FTIR spectra [27], originating presumably from absorbed moisture. Similarly, for PEG capped NPs, the decay times of a sample dispersed in water are similar to those of a powder sample.

Figure 3 reveals that ligands present at the surface exert a pronounced effect on the green-to-red intensity ratio, corresponding to ${}^2\text{H}_{11/2}+{}^4\text{S}_{3/2} \rightarrow {}^4\text{I}_{15/2}$ and ${}^4\text{F}_{9/2} \rightarrow {}^4\text{I}_{15/2}$ transitions, respectively. If the ligands increase population of the red emitting ${}^4\text{F}_{9/2}$ level through multiphonon relaxation of the green emitting ${}^4\text{S}_{3/2}$ level, a decrease of the green-to-red intensity ratio is expected. Thus, this ratio mirrors the contribution of non-radiative relaxation processes, but may also indicate changes in the mechanism of excitation processes. For example, surface ligands may influence the efficiency of cross-relaxation processes between two Er^{3+} ions: $|{}^4\text{I}_{15/2}, {}^4\text{S}_{3/2}\rangle \rightarrow |{}^4\text{I}_{13/2}, {}^4\text{I}_{9/2}\rangle$ and $|{}^4\text{I}_{15/2}, {}^4\text{S}_{3/2}\rangle \rightarrow |{}^4\text{I}_{9/2}, {}^4\text{I}_{13/2}\rangle$.

In Fig.3 the effect of solvent is also clearly noticeable; in all cases the green-to-red intensity ratio is smaller for colloidal dispersion than for solid samples.

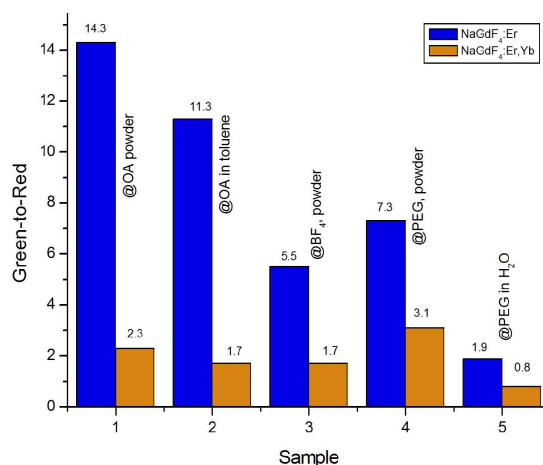


Fig. 3. Green-to-red (${}^2\text{H}_{11/2}+{}^4\text{S}_{3/2}\rightarrow{}^4\text{I}_{15/2}$ to ${}^4\text{F}_{9/2}\rightarrow{}^4\text{I}_{15/2}$) emission intensity ratio for $\text{NaGdF}_4:\text{Er}^{3+}$ (2%) and $\text{NaGdF}_4:\text{Er}^{3+}$ (2%), Yb^{3+} (18%) NPs capped with different ligands measured under direct excitation at 377 nm for solid samples and their colloidal dispersions

Co-doping with Yb^{3+} appears as another important factor influencing emission spectra (Fig. 2) and relative intensities of emission bands (Fig. 3). In the presence of the Yb^{3+} co-dopant the intensity of blue emission at ~ 407 nm, originating from the ${}^2\text{H}_{9/2}$ level, decreases. Addition of Yb^{3+} ions should not influence the multiphonon relaxation rates on Er^{3+} . Then, the observed increase of the relative intensity of green (~ 520 and ~ 540 nm) and red (~ 654 nm) emission as compared to the blue (~ 407 nm) one does not result from more efficient de-excitation of ${}^2\text{H}_{9/2}$, but rather indicates that additional processes populate the ${}^2\text{H}_{11/2}$, ${}^4\text{S}_{3/2}$ and ${}^4\text{F}_{9/2}$ levels more efficiently.

Moreover, in the presence of Yb^{3+} a strong decrease of the green-to-red intensity ratio is observed. Note, that the effect of Yb^{3+} co-doping on this ratio is much larger than those of ligands or solvent.

Most interestingly, for all samples included in Table 1 the decay times of Er^{3+} emissions are longer for Yb^{3+} co-doped NPs than for analogous NPs singly doped with Er^{3+} , regardless of the kind of ligand present on the surface and the form of the studied sample (solid or colloidal dispersion). This observation is to some extent puzzling, since in the presence of Yb^{3+} ions the cross-relaxation processes, e.g. $|(\text{Er})^4\text{S}_{3/2}(\text{Yb})^2\text{F}_{7/2}\rangle \rightarrow |(\text{Er})^4\text{I}_{13/2}(\text{Yb})^2\text{F}_{7/2}\rangle$ are induced as additional de-excitation paths that should decrease the decay time of Er^{3+} . These processes could account for the observed decrease of the green-to-red intensity ratio, but an open question remains why it is not accompanied by the expected decrease of the lifetime of the ${}^4\text{S}_{3/2}$ level. The fact that the lifetimes of this and other emitting levels of Er^{3+} are even longer in the presence of Yb^{3+} ions implies an additional path of population of the ${}^4\text{S}_{3/2}({}^2\text{H}_{11/2})$ and ${}^4\text{F}_{9/2}$ levels. To explain a larger relative contribution of red emission, one must assume that the ${}^4\text{F}_{9/2}$ level is populated more efficiently than ${}^4\text{S}_{3/2}({}^2\text{H}_{11/2})$.

For all the studied samples the green-to-red intensity ratio is smaller for colloidal dispersions than for solid NPs. In addition, the effect of solvent on this ratio is the same for singly Er^{3+} doped NPs as for Yb^{3+} co-doped samples. In colloidal dispersions of OA-capped NPs in toluene the green-to-red intensity ratio decreases for $\text{NaGdF}_4:\text{Er}^{3+}(2\%)\text{@OA}$ and $\text{NaGdF}_4:\text{Er}^{3+}(2\%),\text{Yb}^{3+}(18\%)\text{@OA}$ samples by 1.2 and 1.4 times, respectively, as compared to those of solid state samples. After dispersing the PEG functionalized NPs in water, the ratio decreases by 3.8 times for $\text{NaGdF}_4:\text{Er}^{3+}(2\%)\text{@PEG}$ and by 3.4 times for $\text{NaGdF}_4:\text{Er}^{3+}(2\%),\text{Yb}^{3+}(18\%)\text{@OA}$ NPs. As one may notice, a larger effect is exerted by solvent molecules with more energetic vibrations, owing to larger increase of the non-radiative relaxation rate of the $^4\text{S}_{3/2}$ level or more efficient population of the $^4\text{F}_{9/2}$ level due to other processes.

To explain the above experimental observations one must assume that Yb^{3+} ions participate in population of $(\text{Er})^4\text{S}_{3/2}$ and $(\text{Er})^4\text{F}_{9/2}$ levels after direct excitation of Er^{3+} . The energy transfer from Yb^{3+} to Er^{3+} is an obvious up-conversion process occurring when $\text{Yb}^{3+}(^2\text{F}_{5/2})$ levels are excited with NIR radiation. In the case of direct excitation of Er^{3+} at 377 nm, the cross-relaxation between Er^{3+} and Yb^{3+} must first occur to populate the $^2\text{F}_{5/2}$ level of Yb^{3+} . Then the excited Yb^{3+} ions may transfer the energy back to Er^{3+} ions in a feedback process.

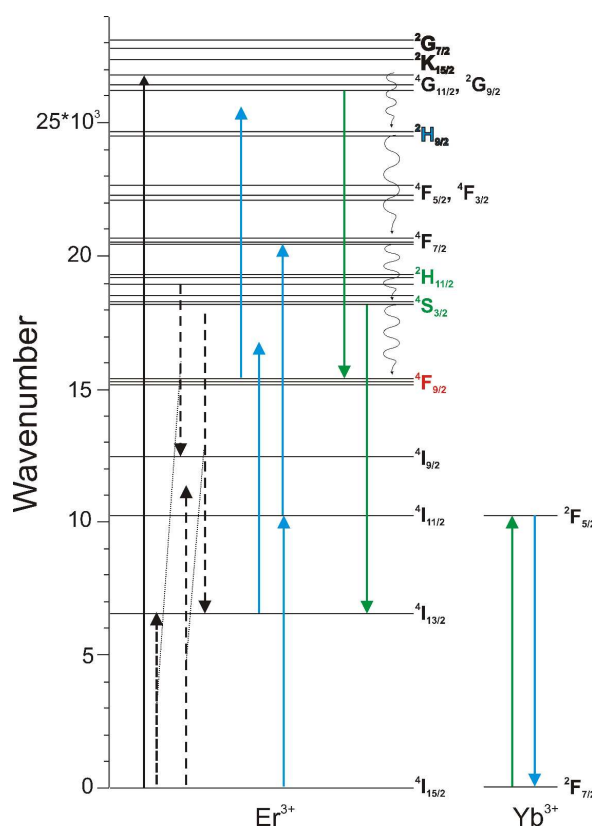


Fig. 4. Schematic energy level diagrams showing possible radiative and nonradiative processes occurring for $\text{NaGdF}_4:\text{Er}^{3+},\text{Yb}^{3+}$ after excitation of Er^{3+} at 377 nm

The proposed mechanism of emission and up-conversion transitions in $\text{NaGdF}_4:\text{Er}^{3+},\text{Yb}^{3+}$ is illustrated schematically in Fig. 4. Excitation energy absorbed by Er^{3+} ions results in the ${}^4\text{G}_{11/2}$ multiplet excited state and then, through phonon assisted relaxation processes, the ${}^2\text{H}_{9/2}$, ${}^4\text{S}_{3/2}$ and ${}^4\text{F}_{9/2}$ levels of Er^{3+} are populated. The phonon-assisted cross relaxation between $\text{Er}^{3+}({}^4\text{S}_{3/2})$ and $\text{Yb}^{3+}({}^2\text{F}_{7/2})$ yields the excited $\text{Er}^{3+}({}^4\text{I}_{13/2})$ and $\text{Yb}^{3+}({}^2\text{F}_{5/2})$ ions. The energy difference of about 1700 cm^{-1} is easily taken up by 3-4 phonons of fluoride host or by even smaller number of phonons if surface ligands with more energetic vibrations are involved. The excited $\text{Yb}^{3+}({}^2\text{F}_{5/2})$ ion can transfer back its energy to a ground state Er^{3+} ion to produce Er^{3+} ion in the excited ${}^4\text{I}_{11/2}$ state. The energy of an excited Yb^{3+} ion can be also transferred to excited $\text{Er}^{3+}({}^4\text{I}_{13/2})$ and $\text{Er}^{3+}({}^4\text{I}_{11/2})$ ions which leads to populating of higher energy ${}^2\text{H}_{9/2}$, ${}^4\text{S}_{3/2}$ and ${}^4\text{F}_{9/2}$ levels. Note, that the energy transfer process leading to population of ${}^4\text{S}_{3/2}$ is a two-photon process when it originates from the ${}^4\text{I}_{11/2}$, but a three-photon process when it originates from the ${}^4\text{I}_{13/2}$ level. The population of ${}^4\text{F}_{9/2}$ is followed by two-photon process irrespective of whether the energy transfer originates from the ${}^4\text{I}_{13/2}$ or ${}^4\text{I}_{11/2}$ level. The difference is that in the latter case the ${}^4\text{F}_{9/2}$ level is populated through multiphonon relaxation of ${}^4\text{S}_{3/2}$. Therefore, the feedback process increases the relative intensity of red emission since the two-photon excitation of the $\text{Er}^{3+}({}^4\text{F}_{9/2})$ is more efficient than the three-photon excitation path into the green emitting $\text{Er}^{3+}({}^4\text{S}_{3/2})$ state. The proposed role of Yb^{3+} ions is additionally proved by the fact that, upon $\text{Yb}^{3+}({}^2\text{F}_{5/2})$ excitation followed by energy transfer to Er^{3+} ions, the contribution of the red emission is usually larger than under direct excitation.

It has been suggested recently [30], that in contrast to the ${}^4\text{S}_{3/2}$ levels which are fed by nonradiative relaxation from ${}^2\text{H}_{9/2}$, the ${}^4\text{F}_{9/2}$ can be efficiently populated directly from ${}^4\text{G}_{11/2}$ in the step including Er-Yb cross-relaxation process: $|(\text{Er})^4\text{G}_{11/2}, (\text{Yb})^2\text{F}_{7/2}\rangle \rightarrow |(\text{Er})^4\text{F}_{9/2}, (\text{Yb})^2\text{F}_{7/2}\rangle$. It should be noticed that this process contributes to enhancement of population of Yb^{3+} excited state under excitation at Er^{3+} with 377 nm wavelength, which increases the probability of the Yb-Er feedback process postulated above. At the same time it additionally increases the red-to-green emission ratio.

The decay times of ${}^4\text{I}_{11/2}$ and ${}^4\text{I}_{13/2}$ levels of Er^{3+} as well as that of ${}^2\text{F}_{5/2}$ level of Yb^{3+} are in milisecond range, much longer than those listed in Table 1. In the sample co-doped with Yb^{3+} these levels participate in a feedback energy transfer process resulting in population of emitting ${}^4\text{S}_{3/2}$ and ${}^4\text{F}_{9/2}$ levels, which explains the observed increase of emission decay times.

In colloidal dispersions the relative population of the ${}^4\text{I}_{13/2}$ state increases owing to more efficient multiphonon relaxation of the ${}^4\text{I}_{11/2}$ levels with participation of high energy vibrations (CH, OH) of solvent molecules. According to the proposed mechanism this should decrease the green-to-red intensity ratio for samples dispersed in solvents, which corroborates well the experimental data.

Hence, one may conclude that the relative population of $\text{Er}^{3+}({}^4\text{I}_{13/2})$ and $\text{Er}^{3+}({}^4\text{I}_{11/2})$ levels appears to be the most important factor determining the green-to-red emission intensity ratio. More efficient multiphonon relaxation (from $\text{Er}^{3+}({}^4\text{I}_{13/2})$) and cross relaxation processes may both contribute to increasing population of the $\text{Er}^{3+}({}^4\text{I}_{13/2})$ state. The increased importance of the former is expected for

organic-ligand capped NPs, whereas the latter are dominant for microscopic samples and explain decrease of the green-to-red intensity ratio with increasing concentration of Er^{3+} [13]. Owing to larger probability of the $|^4\text{S}_{3/2}(^2\text{H}_{11/2}), ^4\text{I}_{15/2}\rangle \rightarrow |^4\text{I}_{9/2}, ^4\text{I}_{13/2}\rangle$ or $|^4\text{S}_{3/2}, ^4\text{I}_{15/2}\rangle \rightarrow |^4\text{I}_{13/2}, ^4\text{I}_{11/2}\rangle$ the cross-relaxation process for samples with higher Er^{3+} concentration, the depopulation of the $^4\text{S}_{3/2}$ is accompanied by increased population of the $^4\text{I}_{13/2}$ level from which the energy is transferred preferentially to the $^4\text{F}_{9/2}$ state.

Suyver et al. [31] have investigated the Er^{3+} emission spectra for microscopic $\text{Er}^{3+}(\text{Yb}^{3+})$ doped NaYF_4 powders and noticed that under direct excitation the effect of cross-relaxation depopulating efficiently the $^4\text{S}_{3/2}$ state in Er^{3+} single doped sample was not so pronounced in the Yb^{3+} co-doped sample. For example for $\text{NaYF}_4:\text{Er}^{3+}(2\%)$, $\text{NaYF}_4:\text{Er}^{3+}(18\%)$ and $\text{NaYF}_4:\text{Er}^{3+}(2\%),\text{Yb}^{3+}(18\%)$ the decay times were 0.36, 0.0026 and 0.14 ms, respectively. The effect was ascribed to strong competition between cross-relaxation on Er^{3+} and energy transfer processes involving Yb^{3+} , but more detailed discussion was not attempted. The effect reported in Ref. [31] seems to be analogous to that described in the present paper. However, for the microscopic powder, even if the emission decay times of Yb^{3+} co-doped sample were longer than expected, they were still shorter ($\tau(^4\text{S}_{3/2}) = 0.14$ ms) or only slightly longer ($\tau(^4\text{F}_{9/2}) = 0.47$) ms than those for only Er^{3+} doped sample ($\tau(^4\text{S}_{3/2}) = 0.36$ ms, $\tau(^4\text{F}_{9/2}) = 0.43$ ms). In contrast, co-doping with Yb^{3+} of nanosized powder causes the emission decay times to become significantly longer than those for the singly Er^{3+} doped sample.

The difference seems to arise from the interplay between different relaxation processes in microsized and nanosized samples. In the microsized material the cross-relaxation appears as the dominant non-radiative process depopulating the $^4\text{S}_{3/2}$ state. The decay time of the $^4\text{F}_{9/2}$ state, is only slightly temperature dependent, which indicates that multiphonon relaxation is suppressed. Co-doping with Yb^{3+} brings in additional cross-relaxation paths, which should further decrease the decay time of the $^4\text{S}_{3/2}$ state, analogously as is observed for samples doped with a higher concentration of Er^{3+} . The energy feedback from Yb^{3+} to Er^{3+} diminishes this effect to some extent, nevertheless, shortening of the decay time of the $^4\text{S}_{3/2}$ emission is observed. On the other hand, in nanosized samples the importance of nonradiative multiphonon relaxation is magnified. The 0.14 ms decay time of the $^4\text{F}_{9/2}$ state in OA-capped NPs is much shorter than for the microsized sample (0.43 ms). Hence, the relative contribution of the feedback energy transfer from Yb^{3+} to Er^{3+} matters much more and a considerable increase of $^4\text{S}_{3/2}$ and $^4\text{F}_{9/2}$ emission decay times is observed in the presence of Yb co-dopant. For nanosized Yb-co-doped samples the decay time of $^4\text{F}_{9/2}$ emission (e.g. 0.14 ms for $\text{NaGdF}_4:\text{Er}^{3+}(2\%),\text{Yb}^{3+}(18\%)@OA$) remains still shorter compared to that of the macro-scale counterpart ($\tau(^4\text{F}_{9/2}) = 0.47$ ms for $\text{NaYF}_4:\text{Er}^{3+}(2\%),\text{Yb}^{3+}(18\%)$ [31]). Similarly, for Er^{3+} only doped nanosized sample the decay time of $^4\text{S}_{3/2}$ (e.g. 0.10 ms for $\text{NaGdF}_4:\text{Er}^{3+}(2\%),\text{Yb}^{3+}(18\%)@OA$) is much shorter than for microscopic sample of the same composition ($\tau(^4\text{S}_{3/2}) = 0.36$ ms [31]). However, for the Yb-co-doped material the decay time of $^4\text{S}_{3/2}$ becomes for nanosized powder even longer (e.g. 0.18

ms for NaGdF₄:Er³⁺(2%),Yb³⁺(18%)@OA) than for its microsized counterpart ($\tau(^4S_{3/2}) = 0.14$ ms for NaYF₄:Er³⁺(2%),Yb³⁺(18%) [31]).

In Ref. [32] the up-conversion mechanism termed the hetero-looping-enhanced energy transfer has been described for silica sol-gel films made with La_{0.45}Yb_{0.50}Er_{0.05}F₃ nanoparticles. The critical step in this mechanism is the cross-relaxation feedback loop. In this step multiphonon-assisted cross-relaxation between Er³⁺(²H_{11/2}) and Yb³⁺(²F_{7/2}) results in the excited Er³⁺(⁴I_{11/2}) and Yb³⁺(²F_{5/2}) ions. Then, the energy is transferred from Yb³⁺(²F_{5/2}) ion to ground state Er³⁺ ion yielding Er³⁺(⁴I_{11/2}) ion. Due to multiphonon relaxation of ⁴I_{11/2} the ⁴I_{13/2} level is populated, which can be then excited to the red emitting ⁴F_{9/2} level through energy transfer upconversion process from excited Yb³⁺ ions. Under excitation at Yb³⁺ ions using NIR radiation the feedback amplification starts to be important only at higher laser power densities, since the substantial population of the reservoir level is required. However, the feedback process between Yb³⁺ and Er³⁺ proposed in [32] is analogous to that observed under direct excitation of Er³⁺.

3.3. Up-conversion spectra

Alteration of multiphonon relaxation processes, due to the presence of surface ligands or solvent molecules, should also affect the up-conversion (UC) spectra obtained under NIR excitation. Although increase of efficiency of non-radiative processes should not influence population of the Yb³⁺(²F_{5/2}) level nor the ²F_{5/2}(Yb)→⁴I_{11/2}(Er) energy transfer rate, it will increase population of the (Er³⁺)⁴I_{13/2} level which in turn should decrease the green-to-red intensity ratio.

Fig. 5a compares the UC spectra recorded for OA- and PEG-capped NaGdF₄:Er³⁺(2%),Yb³⁺(18%) nanoparticles. In accord with expectations the larger contribution of red emission is obviously observed for PEG functionalized NPs, for which multiphonon relaxation is more efficient than for OA-capped NPs.

Fig. 5b shows the log-log plots of UC luminescence intensity as a function of the laser power. For OA capped NPs the slopes indicate that the green (⁴S_{3/2} and ²H_{11/2}) and red (⁴F_{9/2}) UC emissions are two-photon processes. If OA is exchanged with PEG ligand the slope of red ⁴F_{9/2} emission increases from 1.8 to 2.1, whereas the increase of slopes of green ⁴S_{3/2} and ²H_{11/2} emissions is considerably larger, from 2.1 to 2.6 and 2.7, respectively. The UC population of ⁴S_{3/2} and ²H_{11/2} states is a two-photon process involving the ⁴I_{11/2} state for the first excitation step but a three-photon process when involves the ⁴I_{13/2}. In the presence of PEG the larger relaxation rate of ⁴I_{11/2} to ⁴I_{13/2} is expected and, therefore, the increase in slope of green ⁴S_{3/2} and ²H_{11/2} UC emission is observed. UC populating the red emitting ⁴F_{9/2} level remains a two-photon process regardless of whether it originates from the ⁴I_{11/2} or ⁴I_{13/2}. The larger probability of the two-photon process explains relative increase of red ⁴F_{9/2} emission as compared to the green emission (resulting from the less efficient three-photon up-conversion mechanism) for samples with increased population of the ⁴I_{13/2} state (Fig. 5a).

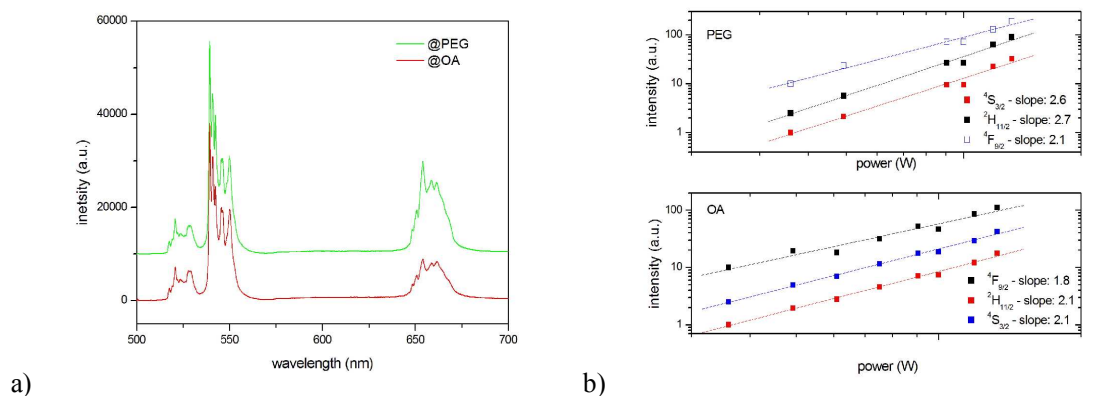


Fig. 5. a) UC emission spectra of NaGdF₄:Er³⁺(2%)Yb³⁺(18%)@OA (i) and NaGdF₄:Er³⁺(2%),Yb³⁺(18%)@PEG NPs under 980 nm excitation; b) power dependence of the ²H_{9/2}→⁴I_{15/2}, ⁴S_{3/2}→⁴I_{15/2} and ⁴H_{9/2}→⁴I_{15/2} transitions of the NaGdF₄:Er³⁺(2%),Yb³⁺(18%)@OA (bottom panel) and NaGdF₄:Er³⁺(2%),Yb³⁺(18%)@PEG (upper panel).

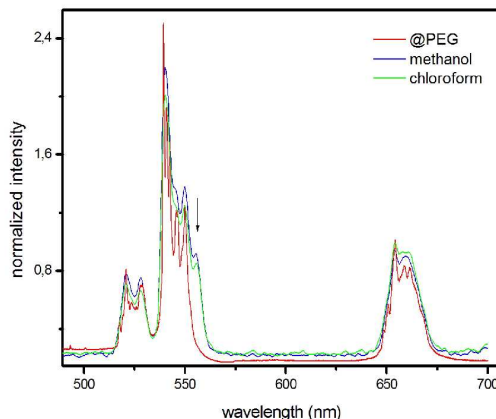


Fig. 6. UC emission spectra of solid NaGdF₄:Er³⁺(2%),Yb³⁺(18%)@PEG NPs (a) and their colloidal dispersions in methanol (b) and chloroform (c) recorded under 980 nm excitation.

Fig. 6 compares UC spectra recorded for PEG-coated solid NaGdF₄:Er³⁺(2%)Yb³⁺(18%)@PEG NPs and their colloidal dispersions in methanol and chloroform. The band at ~556 nm, marked in the figure with an arrow, corresponds to the ²H_{9/2}→⁴I_{13/2} transition. Interestingly, this transition is absent in the spectrum of the solid state sample, but appears in the spectra of sample dispersions in methanol, chloroform, water or other solvents. Similarly, the ~556 nm peak is not observed in the spectrum of solid OA-coated NPs, but becomes visible in the spectra obtained after dispersing the NPs in toluene or chloroform. The ²H_{9/2} level can be populated through the three-photon excitation involving the ⁴I_{11/2} or ⁴I_{13/2} states in the first step. Since solvent molecules increase the multiphonon relaxation rate from ⁴I_{11/2} to ⁴I_{13/2} level, one may conclude from the spectra in Fig. 6 that the up-conversion process leading to population of the ²H_{9/2} multiplet is more efficient if it originates from the ⁴I_{13/2} level.

3.4 Solvent effect.

Since significant differences are observed between spectroscopic properties of powder sample and its colloidal solution, one may also expect a solvent-dependent changes in luminescence of $\text{NaGdF}_4:\text{Er}^{3+}$ and $\text{NaGdF}_4:\text{Er}^{3+}, \text{Yb}^{3+}$ NPs. To verify this supposition the systematic studies were undertaken for NPs colloidal solutions prepared using a variety of solvents. One should be aware, however, that the choice of solvents is limited to those in which NPs form colloidal solutions stable at least for time needed for measurements. Under this criterion 1-octanol, with relative polarity of 0.537, appears as the most polar solvent suitable for dispersion of hydrophobic OA-capped NPs. Besides, the colloidal solutions of OA-capped NPs in hexane (0.009), toluene (0.099), THF (0.207) and chloroform (0.259) were used in measurements. On the other hand, THF came out as the lowest polarity solvent for making stable colloidal dispersion of hydrophilic PEG-capped NPs. The other more polar solvents used for dispersion of these NPs were chloroform, 1-octanol, methanol (0.762) and water (1.0). Thus the relative polarity range of solvents used in the study extends from 0.0 to 0.537 and from 0.207 to 1.000 for OA and PEG capped NPs, respectively. The green-to-red intensity ratio and emission decay times obtained for NPs in different solvents are presented in Fig. 7.

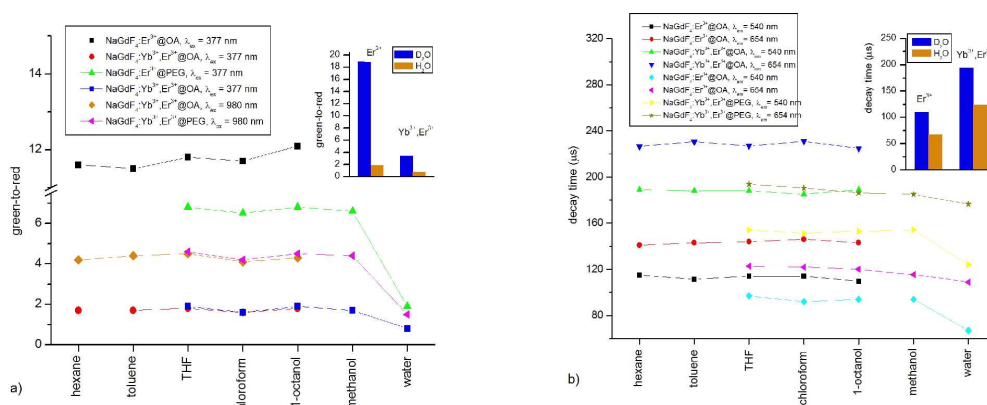


Fig. 7. a) Green-to-red (${}^2\text{H}_{11/2}+{}^4\text{S}_{3/2} \rightarrow {}^4\text{I}_{15/2}$ to ${}^4\text{F}_{9/2} \rightarrow {}^4\text{I}_{15/2}$) emission intensity ratio determined under direct excitation at 377 nm or indirect excitation at 980 nm, and b) decay times of emission ($\lambda_{\text{ex}} = 377$ nm) monitored at 540 or 654 nm, measured for OA- or PEG-capped $\text{NaGdF}_4:\text{Er}^{3+}$ (2%) and $\text{NaGdF}_4:\text{Er}^{3+}, \text{Yb}^{3+}$ (18%) NPs dispersed in different solvents. The insets compares the green-to-red intensity ratio (left panel) or decay time of emission at 540 nm (right panel) for PEG-capped $\text{NaGdF}_4:\text{Er}^{3+}$ (2%) and $\text{NaGdF}_4:\text{Er}^{3+}, \text{Yb}^{3+}$ (18%) NPs dispersed in H_2O and D_2O .

In the case of OA-capped $\text{NaGdF}_4:\text{Er}^{3+}$ or $\text{NaGdF}_4:\text{Yb}^{3+}, \text{Er}^{3+}$ neither green-to-red intensity ratio (Fig. 7a) determined under 377 or 980 nm excitation nor the 540 nm or 654 nm decay times (Fig. 7b) are solvent dependent. This means that OA surface ligands protect the NPs from interactions with solvent molecules. For PEG-capped NPs very similar green-to-red intensity ratios and decay times are observed for dispersions in THF, chloroform, 1-octanol

and methanol. However, markedly different results are obtained for PEG-capped NPs suspended in water. For both NaGdF₄:Er³⁺ and NaGdF₄:Yb³⁺,Er³⁺ the green-to-red intensity ratio is significantly lower in water dispersion compared to other solvents, irrespective of whether the spectra are recorded under direct (377 nm) or indirect (980 nm) excitation (Fig. 7a). The drop of green-to-red intensity ratio is accompanied by decrease of emission decay times, which is more pronounced for the 540 nm than for 654 nm emission. Additional measurements were carried out on PEG-capped NPs dispersed in deuterated water (D₂O). The increase of green-to-red intensity ratio and emission decay time (insets in Fig. 7) observed for D₂O dispersion compared to H₂O dispersion indicates unequivocally that water molecules increase efficiency of non-radiative relaxation processes depopulating the Er³⁺ emitting levels. Analogous isotope effect on green-to-red intensity ratio was observed for ligand-free Yb³⁺/Er³⁺ codoped NaYF₄ NPs [25]. The fact that the solvent effect is observed only in the case of water should be attributed to differences in coordinating ability of solvent molecules. It appears that among solvents used in the study only water molecules are capable to substitute for PEG molecules at NPs surface and thus interact with Ln³⁺ dopant ions.

Conclusions

The emission properties of NaGdF₄ nanoparticles doped with Er³⁺ and/or Yb³⁺ ions and of their colloidal dispersions in different solvents were investigated. Under a direct excitation (377 nm) the surface ligands exert a pronounced effect on Er³⁺ emission decay times, whereas only a minor effect of solvent molecules is observed. On the other hand, both surface ligands and solvents affect significantly the green(⁴S_{3/2}+²H_{11/2})-to-red(⁴F_{9/2}) intensity ratio. It is concluded that the important factor determining this ratio is a relative population of Er³⁺(⁴I_{13/2}) and Er³⁺(⁴I_{11/2}) levels, strongly dependent on the efficiency of multiphonon relaxation processes. Even larger effect on the green-to-red intensity ratio is exerted by the presence of Yb³⁺ co-dopant ions. Moreover, for all studied samples the decay times of Er³⁺ emissions are longer for Yb³⁺ co-doped NPs than for analogous NPs singly doped with Er³⁺. Surprisingly, the decay time of ⁴S_{3/2} becomes even longer for nanosized powder than for its micro-sized counterpart. The proposed mechanism including a feedback energy transfer process from Yb³⁺ to Er³⁺ ions explains the observed elongation of decay times and larger contribution of red emission, due to preferential population of the ⁴F_{9/2} level. The effect of surface ligands manifests itself also in upconversion spectra recorded under NIR excitation (980 nm), since it changes the green-to-red intensity ratio and the dependence of up-conversion emission intensity on excitation power. The increased population of the (Er³⁺)⁴I_{13/2} level, induced by multiphonon relaxation of ⁴I_{11/2}, causes larger contribution of the three-photon process in the energy transfer via up-conversion pathway from Yb³⁺(²F_{5/2}) to Er³⁺(⁴S_{3/2}). It was also observed that the population of the ²H_{9/2} level due to up-conversion energy transfer is more effective for nanoparticle colloidal dispersions than for solid samples. In general, no systematic changes have been observed in emission properties of OA- or PEG-capped NPs dispersed in different polarity solvents, with the exception of water. The water molecules may substitute for PEG-ligands on the NPs surface increasing considerably the multiphonon relaxation of Er³⁺ excited states.

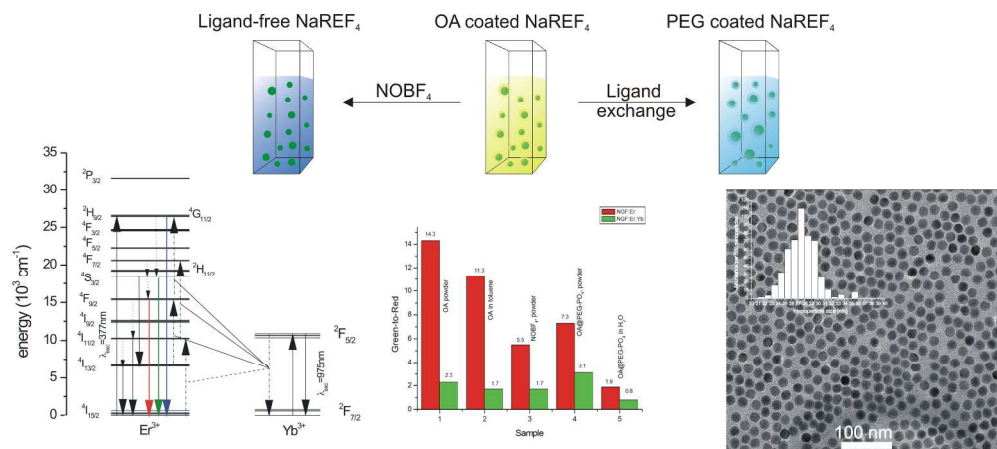
Acknowledgement

Authors acknowledge financial support from the Polish Ministry of Science and Higher Education, Grant N N507 499538.

References

- [1] H. X. Mai, Y. W. Zhang, R. Si, Z. G. Yan, L. D. Sun, L. P. You and C. H. Yan, *J. Am. Chem. Soc.* 2006, **128**, 6426.
- [2] M. Nyk, R. Kumar, T. Y. Ohulchanskyy, E. J. Bergey and P. N. Prasad, *Nano Letters*, 2008, **8**, 3834-3838.
- [3] Z.-L. Wang, J. Hao, H. L. W. Chan, G.-L. Law, W.-T. Wong, K.-L. Wong, M. B. Murphy, T. Su, Z. H. Zhang and S. Q. Zeng, *Nanoscale*, 2011, **3**, 2175-2181
- [4] A. Gnach and A. Bednarkiewicz, *Nano Today*, 2012, **7**, 532-563.

- [5] S. Jin, L. Zhou, Z. Gu, G. Tian, L. Yan, W. Ren, W. Yin, X. Liu, X. Zhang, Z. Hu and Y. Zhao, *Nanoscale*, 2013, **5**, 11910-11918.
- [6] R. Naccache, P. Chevallier, J. Lagueux, Y. Gossuin, S. Laurent, L. Vander Elst, C. Chilian, J. A. Capobianco and M.-A. Fortin, *Advanced Healthcare Materials*, 2013, **2**, 1478-1488.
- [7] F. Vetrone, R. Naccache, V. Mahalingam, C. G. Morgan and J. A. Capobianco, *Advanced Functional Materials*, 2009, **19**, 2924-2929.
- [8] J. Ryu, H.-Y. Park, K. Kim, H. Kim, J. H. Yoo, M. Kang, K. Im, R. Grailhe and R. Song, *J. Phys. Chem. C*, 2010, **114**, 21077-21082.
- [9] G. Chen, T. Y. Ohulchansky, W. C. Law, H. Ågren and P. N. Prasad, *Nanoscale*, 2011, **3**, 2003-2008.
- [10] G. Ren, S. Zeng, J. Hao, *J. Phys. Chem. C*, 2011, **115**, 20141-20147.
- [11] E. N. M. Cheung, R. D. A. Alvares, W. Oakden, R. Chaudhary, M. L. Hill, J. Pichaandi, G. C. H. Mo, C. Yip, P. M. MacDonald, G. J. Stanisz, F. C. J. M. Van Veggel and R. S. Prosser, *Chem. Mater.*, 2010, **22** 4728-4739.
- [12] C. Liu, Z. Gao, J. Zeng, Y. Hou, F. Fang, Y. Li, R. Qiao, L. Shen, H. Lei, W. Yang, M. Gao, *ACS Nano* 2013, **7**, 7227-7240.
- [13] C. Renero-Lecuna, R. Martin-Rodriguez, R. Valiente, J. González, F. Rodriguez, K. W. Krämer and H. U. Güdel, *Chem. Mat.* 2011, **23**, 3442-3448.
- [14] A. Mech, M. Karbowiak, L. Kepiński, A. Bednarkiewicz and W. Strek, *J. Alloys & Comp.* 2004, **380**, 315.
- [15] M. Karbowiak, A. Mech, A. Bednarkiewicz, W. Strek and L. Kepiński, *J. Phys. Chem. Solids*, 2005, **66**, 1008.
- [16] R. Naccache, F. Vetrone, V. Mahalingam, L.A. Cuccia and J.A. Capobianco, *Chem Mater*, 2009, **21** 717-723.
- [17] M. Karbowiak, A. Mech, A. Bednarkiewicz and W. Strek, *J. Alloys & Comp.* 2004, **20**, 321.
- [18] J. Zhang, C. M. Shade, D. A. Chengelis and S. Petoud, *J. Am. Chem. Soc.*, 2007, **129**, 14834-14835.
- [19] J. C. Boyer, M. P. Manseau, J. I. Murray and F. C. J. M. van Veggel, *Langmuir* 2010, **26**, 1157.
- [20] M. Misiak, K. Prorok, B. Cichy, A. Bednarkiewicz and W. Strek, *Opt. Mat.*, 2013, **35**, 1124.
- [21] A. Bednarkiewicz, D. Wawrzynczyk, M. Nyk and W. Strek, *Opt. Mat.* 2011, **33**, 1481.
- [22] D. Wawrzynczyk, M. Nyk, A. Bednarkiewicz, W. Strek and M. Samoc, *J. Lumin.* 2013, 138-144,
- [23] X. Xue, Z. Duan, T. Suzuki, R. N. Tiwari and M. Yoshimura, *J. Phys. Chem. C* 2012, **116**, 22545.
- [24] N. Bogdan, E. M. Rodríguez, F. Sanz-Rodríguez, M. C. Iglesias De La Cruz, Á. Juarranz, D. Jaque, J. G. Solé and J.A. Capobianco, *Nanoscale*, 2012, **4**, 3647-3650.
- [25] N. Bogdan, F. Vetrone, G. A. Ozin and J. A. Capobianco, *Nano Letters*, 2011, **11**, 835-840.
- [26] R. Duncan, *Nature Reviews Drug Discovery* 2003, **2**, 347-360.
- [27] J. Cichos and M. Karbowiak, *Appl. Surf. Sci.* 2012, **258**, 5610.
- [28] J. C. Boyer, M. P. Manseau, J. I. Murray and F. C. J. M. van Veggel, *Langmuir*, 2010, **26**, 1157.
- [29] A. Dong, X. Ye, J. Chen, Y. Kang, T. Gordon, J.M. Kikkawa and C.B. Murray, *J. Am. Chem. Soc.* 2011, **133**, 998
- [30] R. B. Anderson, S. J. Smith, P. S. May and M. T. Berry, *J. Phys. Chem. Lett.* 2014, **5**, 36-42
- [31] J. F. Suyver, J. Grimm, M. K. van Veen, D. Biner, K. W. Krämer and H. U. Güdel, *J. Lumin.* 2006, **117**, 1-12.
- [32] S. Sivakumar, F. C. J. M. Van Veggel and P. S. May, *J. Am. Chem. Soc.* 2007, **129**, 620-625.



232x101mm (300 x 300 DPI)